Fragmentation of $Mg_{24}Y_5$ intermetallic particles in an Mg-Zn-Y alloy during the equal channel angular pressing

Wu, J.; Shi, Q.; Chiu, Y.l.

DOI:
10.1016/j.matchar.2017.04.016

Document Version
Peer reviewed version

Citation for published version (Harvard):
Wu, J, Shi, Q & Chiu, YL 2017, 'Fragmentation of $Mg_{24}Y_5$ intermetallic particles in an Mg-Zn-Y alloy during the equal channel angular pressing', *Materials Characterization*, vol. 129, pp. 46-52.
https://doi.org/10.1016/j.matchar.2017.04.016

Accepted Manuscript

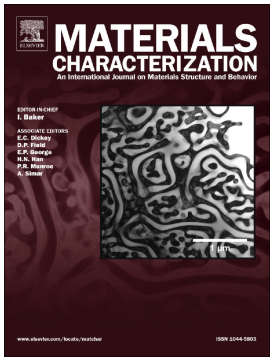

Fragmentation of Mg24Y5 intermetallic particles in an Mg-Zn-Y alloy during the equal channel angular pressing

J. Wu, Q. Shi, Y.L. Chiu

PII: S1044-5803(16)31449-8
DOI: doi: 10.1016/j.matchar.2017.04.016
Reference: MTL 8639

To appear in: *Materials Characterization*

Received date: 31 December 2016
Revised date: 11 April 2017
Accepted date: 12 April 2017

Please cite this article as: J. Wu, Q. Shi, Y.L. Chiu , Fragmentation of Mg24Y5 intermetallic particles in an Mg-Zn-Y alloy during the equal channel angular pressing. The address for the corresponding author was captured as affiliation for all authors. Please check if appropriate. Mtl(2017), doi: 10.1016/j.matchar.2017.04.016

Fragmentation of $Mg_{24}Y_5$ intermetallic particles in an Mg-Zn-Y alloy during the equal channel angular pressing

J. Wu[1*], Q. Shi[2], Y.L. Chiu[1]

[1] School of Metallurgy and Materials, University of Birmingham, Edgbaston, Birmingham, B15 2TT, UK

[2] Department of Materials, Loughborough University, LE11 3TU, UK

[*] Corresponding author. Tel. +44 7549644941. Email address: J.Wu.6@bham.ac.uk (Jing Wu)

Abstract:

Transmission Kikuchi diffraction (TKD) and transmission electron microscopy (TEM) have been used to investigate the fragmentation of $Mg_{24}Y_5$ intermetallic particles in an Mg-Zn-Y alloy during the equal channel angular pressing (ECAP). During the ECAP process, micro-cracks formed in large $Mg_{24}Y_5$ particles and dynamic recrystallised Mg grains were observed inside the crack. The dynamic recrystallisation of the $Mg_{24}Y_5$ also occurred and the particle size has been reduced. The recrystallised $Mg_{24}Y_5$ particles assume either an irregular or necking shape contributing to the dispersion of the small particles. The fragmentation of the $Mg_{24}Y_5$ particles also reduced the grain size of the surrounding magnesium grains. The refinement of the intermetallic particles is expected to improve the strength and ductility of the alloys.

Keywords: $Mg_{24}Y_5$; magnesium alloys; transmission Kikuchi diffraction (TKD); dynamic recrystallisation

Fragmentation of $Mg_{24}Y_5$ intermetallic particles in an Mg-Zn-Y alloy during the equal channel angular pressing

Abstract:

Transmission Kikuchi diffraction (TKD) and transmission electron microscopy (TEM) have been used to investigate the fragmentation of $Mg_{24}Y_5$ intermetallic particles in an Mg-Zn-Y alloy during the equal channel angular pressing (ECAP). During the ECAP process, micro-cracks formed in large $Mg_{24}Y_5$ particles and dynamic recrystallised Mg grains were observed inside the crack. The dynamic recrystallisation of the $Mg_{24}Y_5$ also occurred and the particle size has been reduced. The recrystallised $Mg_{24}Y_5$ particles assume either an irregular or necking shape contributing to the dispersion of the small particles. The fragmentation of the $Mg_{24}Y_5$ particles also reduced the grain size of the surrounding magnesium grains. The refinement of the intermetallic particles is expected to improve the strength and ductility of the alloys.

Keywords: $Mg_{24}Y_5$; magnesium alloys; transmission Kikuchi diffraction (TKD); dynamic recrystallisation

1. Introduction

Intermetallic compounds such as $Mg_{17}Al_{12}$, MgZn and $Mg_{24}Y_5$ can be found in many Mg alloys. Most intermetallics are purposely introduced during the artificial ageing, following high temperature solution treatment, as fine and uniformly dispersed precipitates in an Mg matrix as strengtheners [1] [2]. Intermetallic compounds can also form in cast Mg alloy components. These compounds are relatively large and may act as a source for cracking during services [3] [4] [5]. One such an example is $Mg_{24}Y_5$ widely observed in Mg-Zn-Y alloys [6] [7] [8] [9]. $Mg_{24}Y_5$ assumes the same structure as $Mg_{17}Al_{12}$ (space group $I\bar{4}3m$, Pearson code *cI58*) containing 58 atoms in its unit cell [10]. $Mg_{24}Y_5$ is brittle at room temperature due to the presence of the local icosahedral order, or more generally a local tetrahedral packing of the atomic structure [11], thus the large $Mg_{24}Y_5$ particles are detrimental to the mechanical performance of the alloys and must be refined. Thermo-mechanical processes such as hot extrusion and equal channel angular pressing (ECAP) can effectively refine the intermetallic particles achieving improved mechanical properties [12] [13] [14] [15]. However, the mechanism underlying the refining process that is key to the overall microstructure evolution during the processing remains unclear.

Maghsoudi et al. [16] suggested that the cracking of $Mg_{17}Al_{12}$ particle refined the particles during deformation at 250 °C. Zhou et al. [17] reported a needle-shaped intermetallic phase fragmented through bending and resulted in the fracture of an Al-Si alloy. Another widely observed fragmentation mechanism is through 'necking' [12]. Li. et al. [12] observed barbell-shaped $Mg_{17}Al_{12}$ particles in an extruded AZ91, which was suggested as a result of the necking process where the small $Mg_{17}Al_{12}$ particles can form directly from the divorced eutectic products through the 'necking' of elongated particles. Maghsoudi et al. [16] suggested the necking of the $Mg_{17}Al_{12}$ is related to the strain-induced dissolution of the particles. Liu et al. [18] also suggested

that the strain-induced dissolution played a role in the fragmentation of θ′ particles in an Al-Cu alloy. Despite this, only limited morphological observations have been obtained to understand the fragmentation of the intermetallic particles. Detailed crystallographic information directly correlating the original and the fragmented particles has not been reported.

The lack of evidence concerning the fragmentation process was probably due to the lack of suitable characterisation techniques. TEM offers high spatial resolution crystal orientation determination but is time consuming for studying material fragmentation. Electron backscattered diffraction (EBSD) is useful for providing crystallographic information over a large area but the spatial resolution is limited such that its application to the fragmented small and high strained particles is challenging. Transmission Kikuchi diffraction (TKD, also known as transmission EBSD) has been developed over the last few years [19] [20]. It uses the Kikuchi diffraction pattern formed when electrons transmit through a thin sample in an SEM and requires a small tilting angle (typically 10-20°, rather than the 70° for EBSD), which leads to a significantly improved spatial resolution down to 10 nm [19]. Like conventional EBSD, TKD is able to study a large area of material transparent to the electron beam. Therefore, TKD is a suitable technique to study the fragmentation of intermetallic compound in terms of the spatial resolution and the size of the regions of interest. In this paper, the fragmentation of $Mg_{24}Y_5$ particles in a cast Mg-Zn-Y alloy as the result of ECAP processing has been studied using a combination of TKD and TEM.

2. Experimental

An $Mg_{94}Zn_2Y_4$ (at.%) alloy was prepared using an induction furnace under an argon protective environment from pure magnesium, pure zinc and a Mg-30Y wt. % master alloy. Specimens with dimensions of 10 mm × 10 mm × 20 mm were cut from the as-cast ingot and ECAP

processed for 1, 2 and 3 passes at 300℃ using a 90° die with back pressure. The channel intersection angle Φ and the curvature angle Ψ are 90º and 36º respectively. The samples were rotated 90º in the same direction between two consecutive passes of ECAP.

The deformation microstructure was studied using a Tescan Mira-3 SEM using EDS, EBSD and TKD, and on a JEOL 2100 TEM. Samples for TEM and TKD analysis are 3 mm thin discs prepared by twin-jet electropolishing at -30 °C and 70 V using a solution containing 8.8 g lithium chloride, 19.3 g magnesium perchlorate, 833 mL methanol and 167 mL butoxyethanol. Thin disc samples for TKD were held by a 20° pre-tilted holder. The Kikuchi patterns were collected using a Nordlys EBSD detector and analysed using AZtec software. The EDS information was collected simultaneously using an X-Max SDD detector.

3. Results

Figure 1 shows the typical microstructure of the as-cast $Mg_{94}Zn_2Y_4$ alloy used in the current study. Two types of secondary phases were observed in the Mg matrix, viz. the $Mg_{24}Y_5$ and the long-period stacking ordered (LPSO) phase. In the back-scattered electron imaging mode, the $Mg_{24}Y_5$ phase particles are typically of about 20 μm size and appear in a brighter contrast than the LPSO phase. The magnesium matrix appears darker.

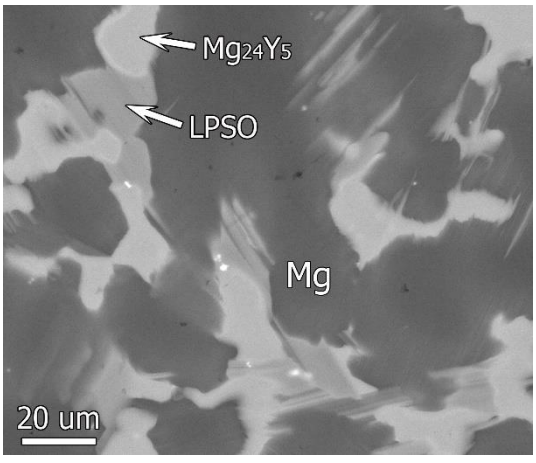

Figure 1 Backscattered SEM image of the as-cast Mg-Zn-Y alloy showing the $Mg_{24}Y_5$ and LPSO phases brighter than the magnesium matrix.

Figure 2 shows the typical morphology of the $Mg_{24}Y_5$ particles after 3 ECAP passes. Figure 2a shows a long particle which has cracked and became thinner in some areas. In the higher magnification image (Figure 2b), fragmented particles (indicated by the arrows) are found in the thin area. The morphology of the thin $Mg_{24}Y_5$ particle area resembles the necking morphologies reported in the literature [12] [16]. Figure 2c shows an area with $Mg_{24}Y_5$ particles of irregular shape detaching from a large $Mg_{24}Y_5$ particle. The higher magnification image (Figure 2d) shows some saw-teeth shaped particles (similar to the micro-sized necking) as indicated by the white arrows. The black arrow indicates a piece of $Mg_{24}Y_5$ particle being torn off the large particle to its right. This detaching particle has an irregular shape and sharp facets.

Small $Mg_{24}Y_5$ particles dispersed in the matrix can be observed, as labelled with I - III in Figure 2. These particles are particle shaped and of about 100 - 200 nm in diameter, smaller than the fragments mentioned. It is believed that these small particles formed during the dynamic recrystallisation of the deformed Mg grains due to the large strain introduced during ECAP.

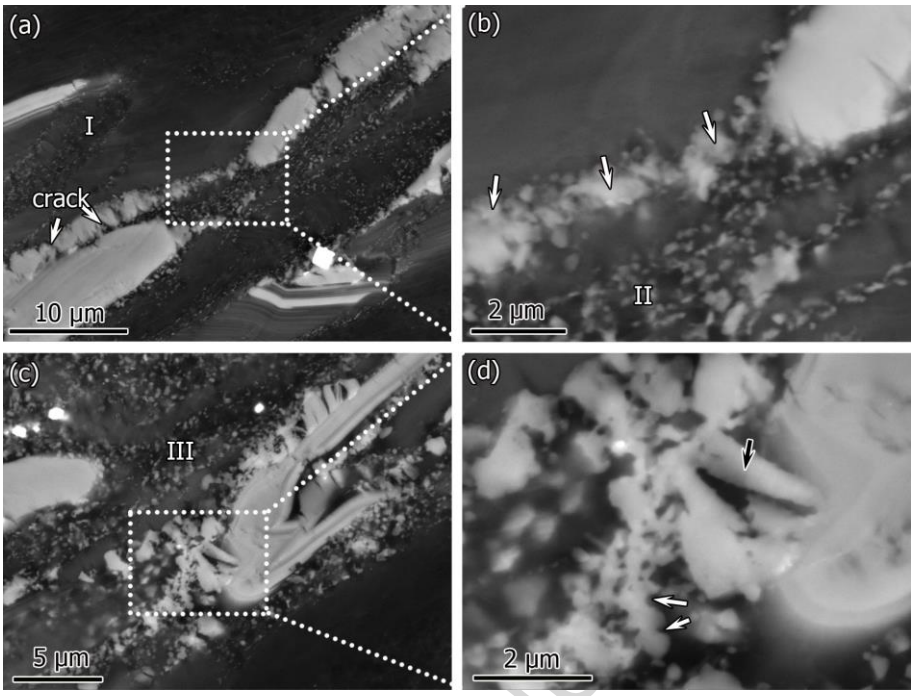

Figure 2 Backscattered electron images obtained from a 3-pass ECAPed sample showing the morphology of the $Mg_{24}Y_5$ phase: (a) (b) cracks and thin area are observed in a long $Mg_{24}Y_5$; (c) (d) small irregular $Mg_{24}Y_5$ particles were torn off from a big particle.

The microstructure of the ECAP processed alloy contains areas with much refined Mg grains, indicating that dynamic recrystallisation (DRX) has occurred during the processing. The typical morphology of a DRXed Mg region is shown in the forward scattered electron (FSE) image in Figure 3a. The FSE image was collected using the diodes located on the sides of the EBSD camera and contains both the Z contrast and the crystallographic orientation information. The EDS map of Y shown in Figure 3b shows that the white particles in Figure 3a have a higher content of Y than the surrounding Mg matrix. The phase map (Figure 3c) confirms that these particles have the same crystallographic structure as the $Mg_{24}Y_5$ phase. Figure 3d shows that the Mg grains and the $Mg_{24}Y_5$ grains have random orientations. These $Mg_{24}Y_5$ particles are largely located on the grain boundaries of the DRXed Mg grains of micron sizes with very few particles in the centre of Mg grains. These particles associated with the DRXed Mg grains and grain

boundaries are smaller and more dispersed than the fragmented $Mg_{24}Y_5$ particles shown in Figure 2.

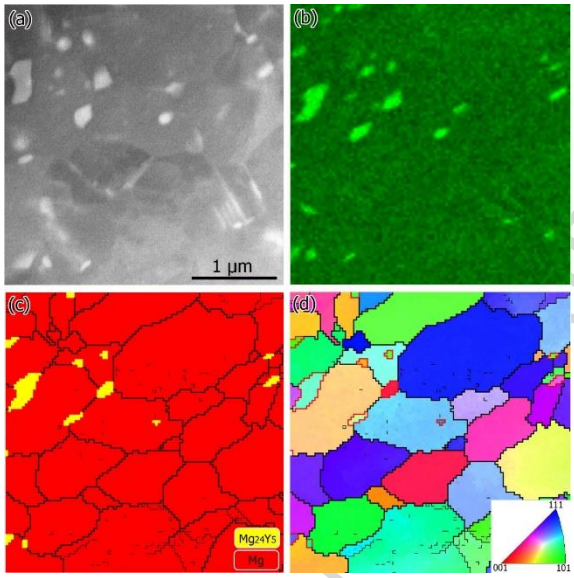

Figure 3 (a) FSE image showing the dispersed $Mg_{24}Y_5$ particles in a DRXed Mg region in the 3-pass ECAPed sample; b) EDS map of Y; c) TKD phase map showing the $Mg_{24}Y_5$ phase is located mainly on the boundaries of the DRXed Mg grains; (d) TKD orientation map of the $Mg_{24}Y_5$ and the DRXed Mg.

Figure 4a shows an SEM image of a 2-pass ECAPed alloy. This area contains lath shaped $Mg_{24}Y_5$ (in grey contrast in the centre of the image) surrounded by LPSO (in brighter contrast) and Mg (in grey). The corresponding phase map of the area is shown in Figure 4b. The $Mg_{24}Y_5$ lath has a few locations which failed in the EBSD indexing, presumably due to the localised strain at these locations. The orientation map in Figure 4c shows that the lower half of the $Mg_{24}Y_5$ lath has an orientation quite different from the top half (misorientation angle of about 6°). Unlike $Mg_{24}Y_5$, no sudden orientation change can be observed in LPSO and Mg due to the deformation.

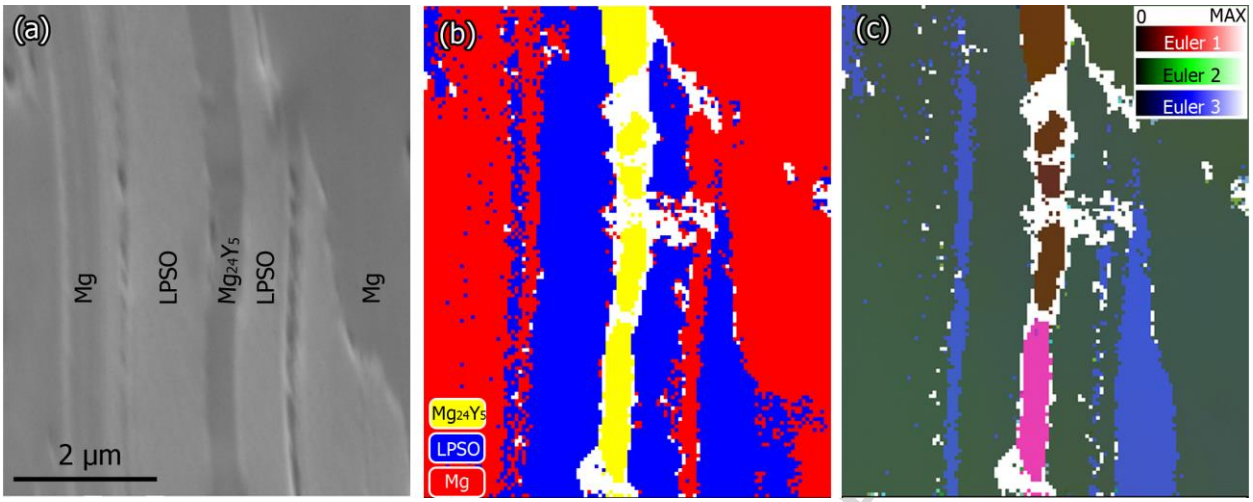

Figure 4 (a) Secondary electron image of 2-pass ECAPed Mg-Zn-Y alloy; (b) Conventional EBSD phase map; (c) Orientation map of the same area.

Figure 5a shows an FSE image of a deformed $Mg_{24}Y_5$ particle in a 2-pass ECAPed sample. Micro-cracks can be observed in the $Mg_{24}Y_5$ particle but not in the surrounding Mg. Figures 5b and c show the TKD orientation maps from the Mg and $Mg_{24}Y_5$ respectively. As indicated by the arrows, small Mg grains are found inside the cracks in the $Mg_{24}Y_5$ particle. The orientations of the small Mg grains are quite different from each other, indicating that these are most likely DRXed grains. The cumulative and nearest-neighbour misorientation profiles along AB line in Figure 5c are plotted in Figure 5d and 5e. The crystal orientation changes gradually within each part of the $Mg_{24}Y_5$ particle. The orientation changes are normally smaller than 2° within each individual piece. Between different parts of the particle, the orientation variations are obviously larger than that inside the individual part and the misorientation angles between neighbouring pieces are less than 10°.

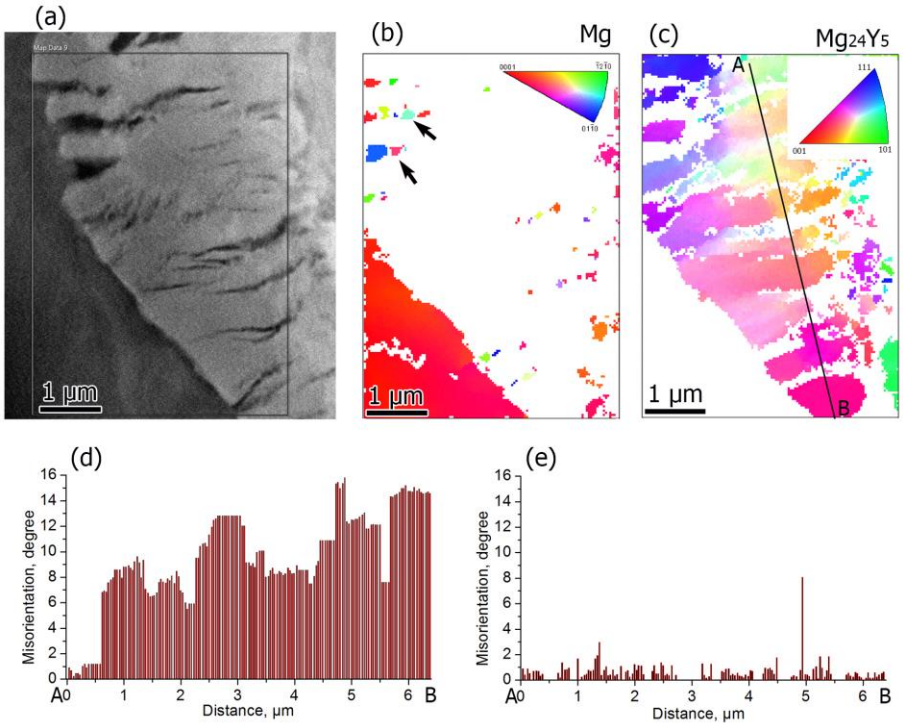

Figure 5 (a) FSE image of a 2-pass ECAPed Mg-Zn-Y alloy showing many cracks in large $Mg_{24}Y_5$ particle; (b) Orientation map of Mg only showing small DRXed grains inside the cracks in $Mg_{24}Y_5$; (c) Orientation map of $Mg_{24}Y_5$ only;(d) cumulative misorientation profile along AB line in Figure 5c; (e) nearest-neighbour misorientation profile along AB line in Figure 5c. Note that after 3 hours of TKD scanning, the orientation maps (b) and (c) slightly drifted compared with the electron image in (a) which was taken at the beginning of the scan.

Figure 6a shows an area containing irregularly shaped bright particles in the 2-pass ECAPed sample. The EDS map of Y (Figure 6b) indicates that Y is rich in the bright particles and the phase map (Figure 6c) confirms that the bright particles are $Mg_{24}Y_5$. The inverse pole figure map (Figure 6d) shows an overall distribution of the orientations of the $Mg_{24}Y_5$ phases. Figure 6e shows the orientation map of the $Mg_{24}Y_5$ and the misorientation angles of grain boundaries are also displayed. The $Mg_{24}Y_5$ particle in the centre of the image has gradually changing orientation and contains low angle grain boundaries with misorientation of about 4° inside. The surrounding

$Mg_{24}Y_5$ particles are composed of small grains of a few hundred nanometres and with random orientations. The misorientation angles between these small grains are typically of 15-60°, which belong to high angle grain boundaries, except some low angle grain boundaries are observed in the blue area (upper right part) and few attached to the large grain (indicated by * followed by the misorientation angle). The blue area contains a mixture of sub-grains and grains with higher misorientation angles of about 11-28°. Compared with the original $Mg_{24}Y_5$ particles which were around 20 μm across and assuming one orientation within each particle in the cast alloy, it is likely that the low angle grain boundaries in the central $Mg_{24}Y_5$ particle are deformed structure and these small $Mg_{24}Y_5$ particles with random orientations are recrystallised grains formed during the ECAP. Figure 6a also shows some 'necking'-like features (i.e. A and B area) in the $Mg_{24}Y_5$ particles and based on Figures 6e, high angle grain boundaries with misorientation angles of 32° and 44° respectively are found in these 'necking'-like features which the neighbouring grains correspond to the recrystallised $Mg_{24}Y_5$ particles.

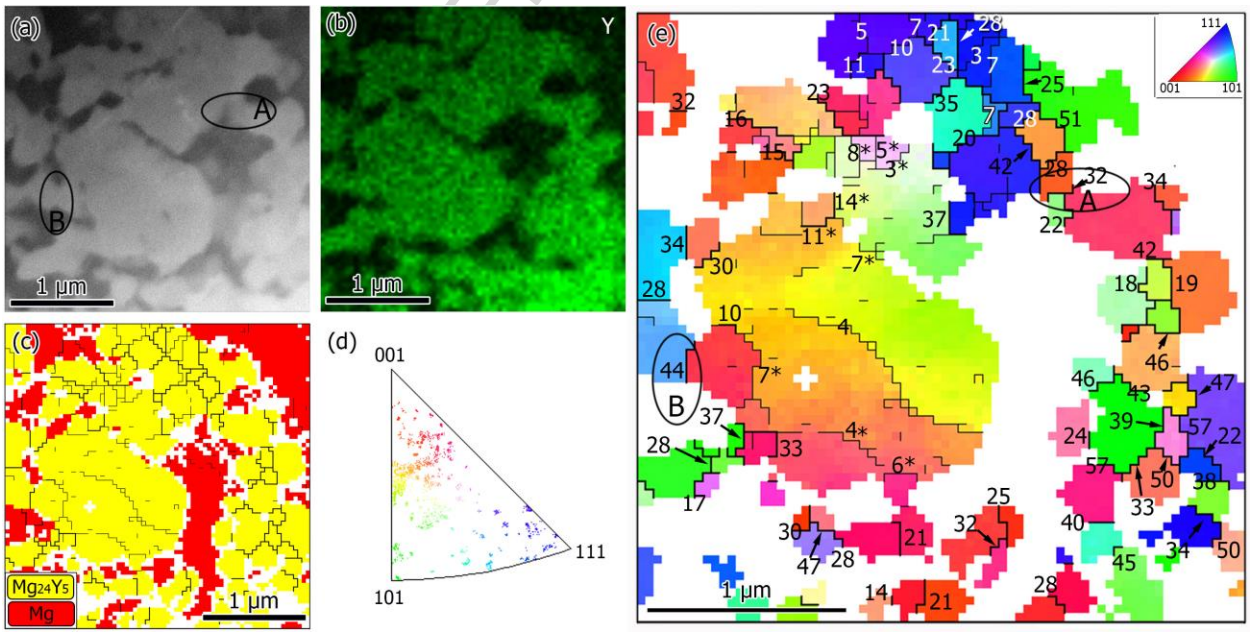

Figure 6 (a) FSE image of 2-pass ECAPed sample; (b) EDS map of Y; (c) phase map with magnesium in red, $Mg_{24}Y_5$ in yellow and unindexed spots in white. The unindexed spots are mainly because Mg and $Mg_{24}Y_5$ may overlap in the TEM foil thickness direction, which causes difficulty indexing the Kikuchi patterns. The thick black lines are grain boundaries with a misorientation larger than 10°; the thin black lines are boundaries where the misorientation lies between 2° and 10°; (d) inverse pole figure of $Mg_{24}Y_5$; (e) magnified orientation map of $Mg_{24}Y_5$ with displayed misorientation angles of the grain boundaries.

Figure 7a shows a TEM bright field image of a deformed $Mg_{24}Y_5$ particle. A crack can be seen in the centre of the image, as indicated by the dashed line. Within the crack, a string of small $Mg_{24}Y_5$ particles are surrounded by Mg. To further characterise the microstructure, the specimen was tilted to obtain changes in the diffraction contrast of the grains (Figures 7b-d). The grains highlighted in red and blue (in Figure 7b) are Mg and $Mg_{24}Y_5$ respectively. Both Mg and $Mg_{24}Y_5$ grains within the crack have different orientations, indicating these are recrystallised grains. This observation agrees with the SEM results shown in Figure 5 where newly formed Mg grains were found in the cracks of a large $Mg_{24}Y_5$ particle.

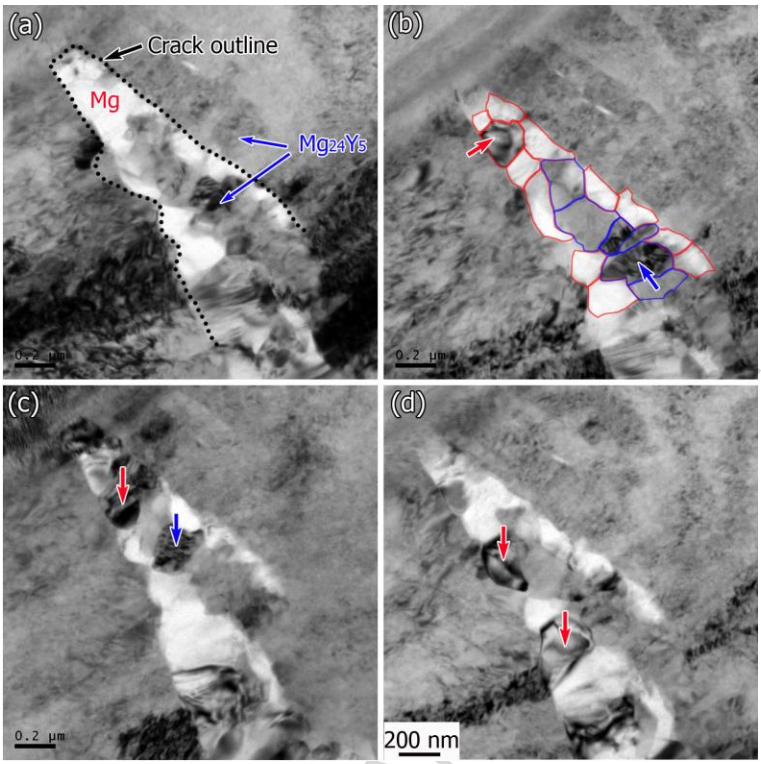

Figure 7 TEM bright field images taken using many beam imaging conditions showing a deformed $Mg_{24}Y_5$ particle with a crack in the centre in a 2-pass ECAPed sample. (a-d) images after tilting showing small grains of Mg and $Mg_{24}Y_5$ inside the crack. The dashed line in Figure 7(a) indicates the outline of the crack. The red and blue grains/arrows indicate the DRXed Mg and $Mg_{24}Y_5$ grains respectively.

4. Discussion

The fragmentation mechanism of intermetallics in a matrix during deformation has been often associated with cracking [16] [17] or 'necking' [12] [16]. Cracking is frequently observed in the current study with the $Mg_{24}Y_5$ particle found near the crack (Figure 5) showing relatively small misorientation angles, indicating the $Mg_{24}Y_5$ particle was directly torn from the bigger particle. Intermetallic compounds are in general brittle with limited formability. The crystal symmetry of the intermetallics is lower than that of conventional metals because of the increased atomic order and thus much larger energy is required to generate a perfect single dislocation. Pugh [21]

introduced the modulus ratio G/B (G: shear modulus, B: bulk modulus) to predict the brittle or ductile behaviour of the material, where a high G/B ratio (larger than 0.57) is associated with brittleness, and vice versa. The G/B ratio of $Mg_{24}Y_5$ is about 0.57 based on the calculated moduli using density functional theory [22], while the G/B ratio of Mg is about 0.33 at room temperature [23]. This indicates that the ductility of $Mg_{24}Y_5$ is much lower than that of Mg at room temperature. The intermetallics such as $Mg_{17}Al_{12}$ generally have higher hardness and Young's modulus than Mg [24] [25], so intermetallics/matrix interface are likely to have stress concentration during ECAP. It is not surprising that micro-cracks are formed inside the $Mg_{24}Y_5$ particles when their deformation is incompatible with the surrounding Mg or LPSO phase. The micro-cracks then efficiently reduce the size of the $Mg_{24}Y_5$ particles.

Regarding the 'necking' mechanism, Li et al [12] claimed that the small $Mg_{17}Al_{12}$ particles observed were formed mostly by necking of the original large $Mg_{17}Al_{12}$ particles and that the necking process resulted in an irregular shape of the $Mg_{17}Al_{12}$ particle. Maghsoudi et al [16] suggested that strain-induced dissolution caused the necking, thinning and separation of the $Mg_{17}Al_{12}$ particles and that small particles deformed at higher temperature and suffering more strain exhibit a more spherical shape. It is obvious that the individual particles or the barbell-shaped particles formed by 'necking' mechanism require a relatively small misorientation between the small particles and the parent grains. However, the 'necking' mechanism has not been observed in the current study. Instead, irregular $Mg_{24}Y_5$ particles after deformation have a similar 'necking' morphology, but this is confirmed to be composed of small DRXed grains. The DRXed particles exhibit relatively spherical shape. This indicates that dynamic recrystallisation of the $Mg_{24}Y_5$ phase is also responsible for the fragmentation.

The dynamic recrystallisation of the pre-existing $Mg_{24}Y_5$ particles are observed both around the deformed grain (Figure 6) and inside a crack (Figure 7). These two scenarios suggest that different dynamic recrystallisation mechanisms are responsible. In general, the recrystallisation mechanism of the secondary phase remains unclear because previous work regarding the dynamic recrystallisation mechanisms has been focused on the single-phase system or the primary phase of a two-phase system [26]. A possible recrystallisation mechanism in Figure 6 is as follows. The DRXed grains with large misorientation angles are located around the deformed particles, and form a similar shape to the necklace grains, as has been often observed in the deformed Mg alloy [27] and NiAl alloy [28]. ECAP process has introduced large strain into the $Mg_{24}Y_5$ especially at the interface between the $Mg_{24}Y_5$ and Mg matrix. Figure 6 shows that sub-grains were developed around the large $Mg_{24}Y_5$ grain and the blue area shows a mixture of the sub-grains and DRXed grains. The sub-grains grew into the DRXed grains observed.

The DRXed $Mg_{24}Y_5$ grains result in different morphologies in the SEM depending on the numbers of attached grains. When two or more $Mg_{24}Y_5$ grains are joined together they show a micro-necking-like shape. The contact region is a weak site which can be easily separated by Mg matrix forming isolated $Mg_{24}Y_5$ particles. This is favourable for further fragmentation of the $Mg_{24}Y_5$ particles. If a single $Mg_{24}Y_5$ grain is replaced by tens of intact grains, then a macro-necking-like feature is observed. If an $Mg_{24}Y_5$ particle is composed of lots of DRXed grains, it exhibits a curved surface with some bulges caused by the small particles.

It is worth noting that small DRXed Mg grains are found inside the crack while the surrounding Mg is still a deformed large grain (Figure 5). In some cases (Figure 7), the DRXed Mg is also accompanied by DRXed $Mg_{24}Y_5$ grains, therefore the fragmented $Mg_{24}Y_5$ particles are separated from the original $Mg_{24}Y_5$ particles. This is probably due to the better formability of Mg than that of $Mg_{24}Y_5$. During the ECAP processing, the high stress squeezes Mg into the cracks. The Mg suffers extremely large strains, which results in small DRXed Mg grains. This indicates that the Mg matrix not only plays an important role in refining the eutectic $Mg_{24}Y_5$, but also fills the cracks and eliminates porosity. As the process continues, eventually $Mg_{24}Y_5$ will break into small separate parts and disperse in the Mg matrix.

In summary, cracking and recrystallisation occur independently and both processes can break down the particles to a smaller size. However, the combination of both cracking and recrystallisation occurs widely and tends to be a more efficient fragmentation process.

5. Conclusions

A fragmentation mechanism has been proposed for eutectic $Mg_{24}Y_5$ intermetallic particles during ECAP. Initially cracks are formed which lead to fragmentation and significantly reduces the size of the $Mg_{24}Y_5$ particles; secondly, dynamic recrystallisation of these intermetallics occurred in the heavily deformed areas, e.g. near the crack. The agglomeration of DRXed $Mg_{24}Y_5$ grains gives rise to necking and thus to a dispersion of small $Mg_{24}Y_5$ particles. Meanwhile, the Mg matrix exhibits better formability than the $Mg_{24}Y_5$, which makes it possible to separate the fragmented $Mg_{24}Y_5$ particles.

Acknowledgement

The authors would like to thank Professors Ian Jones and Mike Loretto for advice and comments on the manuscript. JW is grateful for a Li Siguang PhD Scholarship jointly funded by University of Birmingham and China Scholarship Council. The support from an EPSRC grant (EP/L017725/1) is acknowledged.

References:

[1] Hort N, Huang YD, Kainer KU. *Intermetallics in magnesium alloys.* Adv Eng Mater 2006;**8**(4):235-240.

[2] Nie J-F. *Precipitation and Hardening in Magnesium Alloys.* Metall Mater Trans A 2012;**43**(11):3891-3939.

[3] Lü YZ, Wang QD, Ding WJ, Zeng XQ, Zhu YP. *Fracture behavior of AZ91 magnesium alloy*. Mater Lett 2000;**44**(5):265-268.

[4] Liu WC, Dong J, Song X, Belnoue JP, Hofmann F, Ding WJ, et al. *Effect of microstructures and texture development on tensile properties of Mg–10Gd–3Y alloy*. Mater Sci Eng A 2011;**528**(6):2250-2258.

[5] Gao L, Chen RS, Han EH. *Microstructure and strengthening mechanisms of a cast Mg–1.48Gd–1.13Y–0.16Zr (at.%) alloy*. J Mater Sci 2009;**44**(16):4443-4454.

[6] Luo ZP, Zhang SQ, Tang YL, Zhao DS. *Microstructures of Mg-Zn-Zr-RE alloys with high RE and low ZN contents.* J Alloys Compd 1994;**209**(1–2):275-278.

[7] Rao J, Zhou Y, Yoshimoto S, Yamasaki M, Kawamura Y. *HRTEM study of precipitates in Mg-Zn-Y alloys as cast and after extrusion.* Adv Eng Mater 2005;**7**(7):610-612.

[8] Zhang J, Chen C, Cheng W, Bian L, Wang H, Xu C. *High-strength $Mg_{93.96}Zn_2Y_4Sr_{0.04}$ alloy with long-period stacking ordered structure.* Mater Sci Eng A 2013;**559**(0):416-420.

[9] Inoue A, Kawamura Y, Matsushita M, Hayashi K, Koike J. *Novel hexagonal structure and ultrahigh strength of magnesium solid solution in the Mg-Zn-Y system.* J Mater Res 2001;**16**(7):1894-1900.

[10] Bonhomme F, Yvon K. *Synthesis and crystal structure refinement of cubic $Mg_{6.8}$ Y.* J Alloys Compd 1996;**232**(1–2):271-273.

[11] Ragani J, Donnadieu P, Tassin C, Blandin JJ. *High-temperature deformation of the γ-$Mg_{17}Al_{12}$ complex metallic alloy.* Scripta Mater 2011;**65**(3):253-256.

[12] Li Z, Dong J, Zeng XQ, Lu C, Ding WJ. *Influence of $Mg_{17}Al_{12}$ intermetallic compounds on the hot extruded microstructures and mechanical properties of Mg–9Al–1Zn alloy.* Mater Sci Eng A 2007;**466**(1–2):134-139.

[13] Minárik P, Král R, Pešička J, Daniš S, Janeček M. *Microstructure characterization of LAE442 magnesium alloy processed by extrusion and ECAP.* Mater Charact 2016;**112**:1-10.

[14] Zeng X, Zhang Y, Lu C, Ding W, Wang Y, Zhu Y. *Precipitation behavior and mechanical properties of a Mg–Zn–Y–Zr alloy processed by thermo-mechanical treatment.* J Alloys Compd 2005;**395**(1–2):213-219.

[15] El-Morsy A, Ismail A, Waly M. *Microstructural and mechanical properties evolution of magnesium AZ61 alloy processed through a combination of extrusion and thermomechanical processes.* Mater Sci Eng A 2008;**486**(1–2):528-533.

[16] Maghsoudi MH, Zarei-Hanzaki A, Abedi HR, Shamsolhodaei A. *The evolution of γ-$Mg_{17}Al_{12}$ intermetallic compound during accumulative back extrusion and subsequent ageing treatment.* Philos Mag 2015;**95**(31):3497-3523.

[17] Zhou J, Duszczyk J, Korevaar BM. *Structural development during the extrusion of rapidly solidified Al-20Si-5Fe-3Cu-1Mg alloy.* J Mater Sci 1991;**26**(3):824-834.

[18] Liu Z, Bai S, Zhou X, Gu Y. *On strain-induced dissolution of θ′ and θ particles in Al–Cu binary alloy during equal channel angular pressing.* Mater Sci Eng A 2011;**528**(6):2217-2222.

[19] Keller RR, Geiss RH. *Transmission EBSD from 10 nm domains in a scanning electron microscope.* J Microsc 2012;**245**(3):245-251.

[20] Trimby PW. *Orientation mapping of nanostructured materials using transmission Kikuchi diffraction in the scanning electron microscope.* Ultramicroscopy 2012;**120**(0):16-24.

[21] Pugh SF. *XCII. Relations between the elastic moduli and the plastic properties of polycrystalline pure metals.* The London, Edinburgh, and Dublin Philosophical Magazine and Journal of Science 1954;**45**(367):823-843.

[22] Wang N, Yu W-Y, Tang B-Y, Peng L-M, Ding W-J. *Structural and mechanical properties of $Mg_{17}Al_{12}$ and $Mg_{24}Y_5$ from first-principles calculations.* J Phys D: Appl Phys 2008;**41**(19):195408.

[23] Friedrich HE, Mordike BL, *Magnesium Technology: Metallurgy, Design Data, Automotive Applications* 2006: Springer Berlin Heidelberg.

[24] Mathur HN, Maier-Kiener V, Korte-Kerzel S. *Deformation in the γ-$Mg_{17}Al_{12}$ phase at 25–278 °C.* Acta Mater 2016;**113**:221-229.

[25] Haghshenas M, Bhakhri V, Oviasuyi R, Klassen RJ. *Effect of temperature and strain rate on the mechanisms of indentation deformation of magnesium.* MRS Commun 2015;**5**(03):513-518.

[26] Doherty RD, Hughes DA, Humphreys FJ, Jonas JJ, Jensen DJ, Kassner ME, King WE, McNelley TR, McQueen HJ, Rollett AD. *Current issues in recrystallization: a review.* Mater Sci Eng A 1997;**238**:219-274.

[27] Ion SE, Humphreys FJ, White SH. *Dynamic recrystallisation and the development of microstructure during the high temperature deformation of magnesium*. Acta Metall 1982;30: 909-1919.

[28] Ponge D, Gottstein G. *Necklace formation during dynamic recrystallization: mechanisms and impact on flow behaviour*. Acta Mater 1998;**46**: 69-80.

Highlights:

1. Transmission Kikuchi diffraction was used to study the fragmentation of the $Mg_{24}Y_5$.

2. During deformation, micro-cracks and dynamic recrystallisation occur in $Mg_{24}Y_5$.

3. The dynamic recrystallisation reduced the size of the $Mg_{24}Y_5$ particles.

4. The fragmentation of $Mg_{24}Y_5$ also reduced the grain size of the surrounding Mg.